FEATURE ARTICLE

Electron Transmission through Molecular Layers

R. Naaman* and A. Haran

Department of Chemical Physics, the Weizmann Institute of Science, Rehovot 76100, Israel

A. Nitzan, D. Evans,† and M. Galperin

School of Chemistry, Tel Aviv University, Tel Aviv 69978, Israel

Received: December 4, 1997; In Final Form: March 10, 1998

This article discusses general issues associated with electron transmission through thin molecular films. On the experimental side, we emphasize recent investigations of photoemission through organized organic films adsorbed on metal surfaces. Theoretical and numerical approaches to transmission and tunneling through such films are discussed. We focus on the relation between the structure of the film and its transmission properties. In the experimental work, these are controlled by varying the organic layer, by changing its thickness and by inducing disorder via thermal heating and by depositing mixtures of two molecular types. In numerical simulations of simple model systems, we consider the dimensionality of the process, effect of molecular ordering, and relation between electronic band structure in the film and its transmission properties. It is shown that electron transmission through thin molecular layers constitutes a sensitive tool for investigating molecular film properties in addition to providing a convenient prototype system for the study of electron transport in molecular electronic devices.

1. Introduction

Electron transfer, a fundamental chemical process underlying all redox reactions, has been under experimental and theoretical study for many years.[1] The process involves a donor and acceptor pair, a solvent affecting fluctuations in the donor and acceptor electronic energies, intramolecular nuclear modes of the donor and the acceptor, and the electronic coupling responsible for the transfer. The different roles played by these aspects-of the process and the way they affect qualitative and quantitative aspects of the electron transfer process have been repeatedly discussed in the past half-century. These kinds of processes, which dominate electron transitions in molecular systems, are to be contrasted with electron transport in the solid state−metals and semiconductors. These two domains of physical/chemical phenomena overlap in the field of electrochemistry, where the fundamental process is interfacial electron transfer between a molecule or an ion in solution and an electronically conducting solid. In recent years we have seen the emergence of a new field of study, involving molecular "wires" connecting metal or semiconductor contacts.[2,3] Here the traditional molecular view of electron transfer between donor and acceptor species gives rise to a novel view of the molecule as a current-carrying conductor, and observables such as electron-transfer rates and yields are replaced by the conductivities of such molecular junctions or, more generally, by a current−voltage relationship.

This feature article deals with a related but somewhat different type of electron-transfer process: the transmission of electrons through thin molecular films adsorbed on suitable substrates. Such processes can be realized in several ways. A typical experiment of this type is electron photoemission through adsorbed molecular layers. Here the signal is the (angle- and velocity-resolved) transmitted electron flux as a function of incident photon energy, molecular film thickness, adsorbate, and substrate types and temperature. A closely related experiment is low-energy electron transmission (LEET)[4] where a monochromatic electron beam hits an adsorbed molecular layer from the vacuum side; the transmission is monitored via the current generated in the conducting substrate. The same experimental setup can be used to study reflection. Both transmission and reflection are studied as functions of the incident electron energy, substrate type, and characteristics of the molecular layer. Relevant information for lower energy regimes may also be obtained by monitoring current vs voltage in contacts made of two metal electrodes separated by a molecular spacer[5] or in scanning tunneling microscopy, STM,[6] where a surface scan of the current vs bias voltage can be measured as a function of film thickness (i.e., tip−substrate separation). An older technique, inelastic tunneling spectroscopy,[7] is used to obtain information on nuclear motions in the barrier by observing their effect on the electron-tunneling process.

The purpose of the experimental work described below is to study electron transmission through adsorbed molecular layers and the physical factors controlling it: the initial energy input (photon energy in case of photoemission, electron beam energy in LEET experiments), the substrate work function as affected by the adsorbed molecular layer, the chemical nature of the adsorbed layer, its thickness, structure, and the temperature. We

† Present address: Department of Chemistry, University of New Mexico, Albuquerque, NM 87131.

S1089-5647(98)00427-1 CCC: $15.00
Published on Web 04/22/1998

note that photoemission, which is the main tool used by our group, and LEET supplement each other in an interesting way: in LEET we control the energy and direction of the incident electron beam, while in photoemission we can resolve the energy and direction of the transmitted signal. Both types of experiments look at electron transmission through thin films at positive (relative to vacuum) electron energies. From the theoretical point of view both processes, as well as the other electron transmission processes mentioned above, are controlled by similar physical factors: those which affect the magnitude of the electronic coupling and determine the transmission probability.

From the theoretical viewpoint, our aim is to understand the interrelationship between the layer structure and chemical composition and between its transmission properties. In particular we will argue that besides specific effects related to the detailed properties of particular layers and molecules, there are some generic issues: order vs disorder, effects of band structure and band gaps in the layer, resonance effects, and the relation between different observables. Understanding of these generic effects on electron transmission is the purpose of the theoretical work described below.

In the next sections experimental and theoretical backgrounds are given followed by descriptions of the experimental and computational methods. In sections 6 and 7 the experimental and numerical results are presented, respectively, followed by the discussion.

2. Experimental Background

The effect of adsorbates on photoelectrons emitted from surfaces has been studied for almost a century.[8,9] These experiments were partially motivated by their practical ramifications whereby the surface work function was modified by the adsorbate.[10,11] Recently, with the development of tunable UV light sources, the field of energy-resolved photoelectron spectroscopy has been developed.[12] The photoelectron energy distribution was measured for electrons produced from a Pt(111) surface covered with several layers of water.[13] It was found that the transmission probability decreases exponentially with increasing number of water layers but is independent of the energy of the electrons. Similarly, LEET experiments were performed on solid water.[14] Less attention has been given to the effect of organic adsorbate on the efficiency of photoelectron emission, and only a few works on the subject have been published.[15,16]

Electron transmission through organic thin films condensed on metal substrates has been investigated in the past mainly by low-energy electron-transmission (LEET) spectroscopy.[17] It was suggested that for films of saturated hydrocarbon chains of various lengths, the low-energy electron transmission is governed mainly by the film electronic band structure.[18,19] In other LEET studies, it has been established that the conduction band in many alkane layers is at about 0.2−0.8 eV above the vacuum level.[20] Also in the case of ordered rare gas and other simple molecular layers, the transmission,[21] as well as the reflection[22] were found to correlate strongly with the band structure of the corresponding crystals.

Organized organic thin films (OOTFs), which are the subject of our present experimental studies, have the advantage of being well-defined in terms of orientation and packing. Owing to their nature, their thickness can be modified in a controlled manner with a single-layer resolution. Electron-transport properties of such films have been studied extensively in the past.[23,24] In those studies, the current versus voltage applied between electrodes with OOTF spacers was measured. By the nature of such experiments, the dependence of the process on the electron energy cannot be monitored. Moreover, such processes involve in principle both minority and majority carriers and are therefore not easy to control and to interpret. Finally, the effect on the film resistivity of possible pinholes in the organic film makes quantitative analysis uncertain. The photoemission work described below overcomes some of these difficulties by focusing on electrons as majority carriers and by providing the possibility for energy resolution in the outgoing beam.

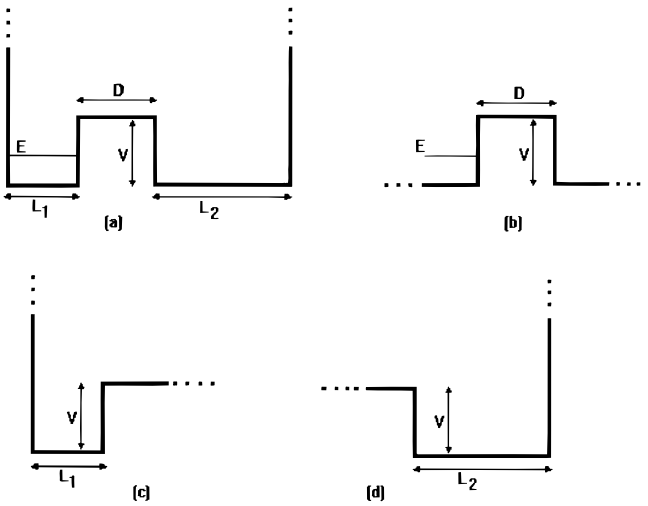

Figure 1. (a) A double well and (b) its barrier part, used in the text to demonstrate the relation between the decay of a prepared state and a scattering process. (c) and (d) are the left- and right-side structures whose eigenstates are used as zero-order states in the treatment of the transmission problem.

3. Theoretical Background

While the experimental part of the present article focuses on photoemission through adsorbed molecular layers, all electron-transfer and -transmission phenomena mentioned in section 1 are controlled by similar physical factors. This section briefly outlines the corresponding theoretical approaches and the relations between them. Broadly speaking we may distinguish between processes for which lifetimes, rates, (more generally the time evolution), or yields are the main observables and those which monitor *fluxes* or *currents*. The latter group may be further divided into processes that measure current−voltage relationships, mostly near equilibrium, and those that monitor the nonequilibrium flux. The latter may be observed as a transient following optical pulse excitation or (ideally) as a steady-state signal caused by a constant incident photon or electron beam.

The relation between these different observables is easily illustrated using the simple well/barrier model shown in Figure 1. Figure 1a depicts a simple model of an asymmetric double well, characterized by two rectangular wells bounded from the outside by infinite potential walls and separated from each other by a rectangular barrier of height V and width D. Viewed as a model for an initial value problem, the system is assumed to be at time $t = 0$ in an eigenstate of the well depicted in Figure 1c, which is identical to the left well of Figure 1a except that the barrier is continued to infinity on the right. This initial state interacts with states associated with the well on the right, which may be approximated by eigenstates of the well of Figure 1d. We expect an exponential decay, $\exp(-\Gamma t)$, of the initial state in the limit where the width, L_2, of the right well becomes

infinitely large so that the eigenstates of the corresponding well in Figure 1d constitute a continuum. Figure 1b shows the equivalent problem of a barrier identical to that in Figure 1a, separating two infinite half-spaces—a typical model of a scattering process. An incident particle of energy E, represented by an incoming wave function $\exp(ikx)$ ($k = \hbar^{-1}(2mE)^{1/2}$, where m is the electron mass) is scattered such that its outgoing components are $A_t(E)\exp(ikx)$ to the right and $A_r(E)\exp(-ikx)$ to the left of the barrier. The simplest observable is the transmission coefficient $T(E) = |A_t(E)|^2$. When Figure 1b represents a model of a junction connecting two ideal one-dimensional conductors which lead into electrons reservoirs characterized by electron chemical potentials μ_1 on the left and μ_2 on the right ($\mu_2 - \mu_1 = -e\Delta\Phi$ where e is the electron charge and $\Delta\Phi = \Phi_2 - \Phi_1$ is the electrostatic potential difference between the reservoirs), the transmission coefficient determines the conductivity of the junction in the linear response regime according to the Landauer formula[25,26] (for temperature $T = 0$, i.e. $\mu = E_F$)

$$G = \frac{I}{e\Delta\Phi} = \frac{e^2}{\pi\hbar}T(E_F) \tag{1}$$

where I is the current induced by the potential difference $\Delta\Phi$. The three-dimensional analog of this result is given by the multichannel Landauer formula[27]

$$G = \frac{e^2}{\pi\hbar}N(E_F) \tag{2}$$

where $N(E)$ is the so-called cumulative reaction probability at energy E. In terms of the transmission amplitudes, $S_{if}(E)$, between an incident state i and a transmitted state f, both of energy E, the cumulative reaction probability is

$$N(E) = \sum_i \sum_f |S_{if}(E)|^2 \tag{3}$$

Note that S_{if} is in fact just the scattering matrix between the incoming and transmitted outgoing free electron states i and f.

Returning to the time evolution of an initially prepared state i on the left, we consider the limit $L_2 \rightarrow \infty$, so that the time evolution is characterized by an exponential decay. The decay rate Γ_i is given by the golden rule formula

$$\Gamma_i = 2\pi\sum_f |V_{if}|^2\delta(E_f - E_i) \cong 2\pi(|V_{iF}|^2\rho_F)_{E_f=E_i} \tag{4}$$

where F denotes the continuum of states $\{f\}$, eigenstates of the right well, characterized by the density of states ρ_F, and where we have assumed that $V_{if} = V_{iF}$ is independent of the level f in the group of states that conserve energy. (The latter assumption is rigorously valid in the one-dimensional model of Figure 1a, while greater care is needed in the analogous three-dimensional problem). The states $\{i\}$ and $\{f\}$ are eigenstates of the zero-order Hamiltonians associated with the potentials of parts c and d of Figure 1, respectively, and the use of the weak coupling expression 4 implies that we consider only energies small enough relative to the barrier height V. In their respective wells these states have the general form

$$\psi_{i(f)}(x) = 2C_{i(f)}\sin[k_{i(f)}(x - x_{1(2)})] \tag{5}$$

where x_1 and x_2 are, respectively, the left edge of the left well and the right edge of the right well and where the parameters k_i and k_f and the normalization parameters C_i and C_f depend on the sizes of the corresponding wells. As they continue into the barrier region these states decay exponentially with the distance from the corresponding barrier edge. Obviously these two groups of states are not orthogonal to each other even though orthogonality exist within each group. It may be shown that the effective coupling matrix element V_{if} to be used in (4) is given by

$$V_{if} = \langle i|H|f\rangle - E_i\langle i|f\rangle \tag{6}$$

Now, evaluating Γ_i for the model depicted in Figure 1a (with $L_2 \rightarrow \infty$), then taking the limit of the resulting rate as $L_1 \rightarrow \infty$, we may write the resulting expression in terms of the transmission probability. The result is[28]

$$\Gamma_i = |C_i|^2\frac{\hbar^2 k_i}{m}T(E_i) \tag{7}$$

Note that this result could be obtained simply by postulating that the decay rate Γ and the transmission probability T are related by $\Gamma/\hbar = \text{flux}\cdot T$, together with the observation that the flux impinging on the barrier is $|C_i|^2\cdot(\hbar k_i)/m$. In the three-dimensional case one has to sum over all final "decay channels", i.e. all possible directions of the transmitted electron. In this case an equation similar to (7) is obtained, in which the transmission probability $T(E)$ is replaced by the sum of transmission probabilities into all final states, i.e., all final transmitted directions:

$$\Gamma_i = |C_i|^2\frac{\hbar^2 k_i}{m}\sum_f |S_{if}(E_i)|^2 \tag{8}$$

Finally consider a photoemission or a LEET experiment. The simplest models for this experimental situation is a nonequilibrium steady-state distribution of electrons incident on the barrier from, say, the left. In a LEET experiment the initial electron state may be sharply defined in terms of energy and direction and the monitored signal corresponds to all possible final states. The monitored signal is therefore proportional to $\sum_f |S_{if}(E_i)|^2$. In the photoemission experiment the initial electron states span a broad energy range between zero and up to $\hbar\omega - E_F$, where ω is the exciting photon frequency and E_F is the substrate's work function. However, energy selection can be affected by resolving the energy of the transmitted electron. Assuming that the optical excitation generates an electron distribution that is uniform in angular space, the monitored signal is proportional to $\sum_i |S_{if}(E_f)|^2$. Thus, the two types of experiments convey equivalent information and are related to the transmission probability of the "one-to-all" type. Note, however, that in reality the angular distribution of the photoelectrons is not necessarily isotropic, though this probably holds for the low-energy secondary electrons. For primary electrons this distribution is determined by the photoexcitation conditions,[29] providing another experimentally controlled variable.

We thus see that photoemission through adsorbed molecular layers, as well as the other electron-transfer and -transmission processes discussed above, are controlled by electron-transmission probabilities through the corresponding barriers, e.g., the simple square barrier of Figure 1b. Evaluating such probabilities for realistic barriers is obviously much more difficult, and some numerical approaches are discussed below.

4. Experimental Methods

We have discussed above the interrelation between different observables associated with electron transmission. Here we

focus on the experiments carried out in our group: photoemission through organized organic thin films (OOTFs).

Film Preparation and Characterization. Several types of OOTFs were prepared. We used, for the work described here, Langmuir Blodgett[30] films. The LB films were deposited using a Nima 611, GB trough and transferred either to a quartz microscope slide coated with 150 nm thick silver or gold films or to a silicon wafer (100). Three organic molecules were used, cadmium stearate (CdSt), $(CH_3(CH_2)_{16}COO^-)_2Cd^{2+}$, and cadmium salts of arachidic and brassidic acids, (Cdar) = $(CH_3(CH_2)_{18}COO^-)_2Cd^{2+}$ and (CdBr) = $(CH_3(CH_2)_7CH{=}CH(CH_2)_{11}COO^-)_2Cd^{+2}$. All acids were dissolved in chloroform (1 mg/mL) and then spread on aqueous solution of 0.001 M $CdCl_2$. The pH of the solution was balanced at 8.5 by small amount of ammonia. At this pH the films are transferred. The depositions were performed at temperature of 20 °C and surface pressure of 28 mN/m, at a low lift speed of 1 cm/min.

The quality of the LB layers was determined by the transfer ratio from the trough, by ellipsometric studies that probe the thickness of the layers, and by IR spectroscopy. For successfully deposited films, the contact angle with water was 111−113°. The ellipsometric data for CdSt and CdBr show that the thickness of each single layer is about 2.40 ± 0.05 nm, independent of the film composition. This number indicates that the CdBr layers, despite being slightly longer than CdSt, are tilted relative to the surface normal, and therefore the thickness of the layers of the two types of film are almost identical. Atomic force microscopy studies confirmed the results obtained from ellipsometry. Layers in which there was a 1:1 mixture of the two molecules were also produced and probed by the same methods, and their quality was found to be the same as that of the other layers.[31] From other studies[32] it is known that the 1:1 mixed layer is homogenous, and no domains are formed.

For each film, the grazing angle Fourier transform infrared (FTIR) spectrum was measured and the intensities of the C−H stretching bands (CH_3 asymmetric, CH_2 asymmetric, and CH_2 symmetric at 2958, 2917, and 2849 cm^{-1}, respectively) were monitored. In addition atomic force microscopy (AFM) measurements were performed on the films. Usually the films have roughness similar to that of the original clean substrate.[33]

Photoelectron Energy Distribution Measurements. Two experimental setups were used for obtaining the transmission function of photoelectrons through the OOTFs. In the first, described in ref 34, a commercial UPS system was utilized (Kratos Analytical, AXIS-HS). The UV source was a helium lamp emitting mainly at the He(I) line (21.21 eV), owing to the He pressure conditions—$0.6-1.0 \times 10^{-7}$ mbar. In order to minimize damage to the organic film, the current through the lamp was reduced to the minimum required to obtain stable UV radiation (30 mA). We examined the effect of OOTF on the secondary electron emission (SEE) peak of the silver substrate. Each set of measurements was comprised of measurement of two samples; a Cdar-coated silver film and a bare silver film as a reference. To account reliably for the peak shape of the very slow (secondary) electrons, special experimental conditions were chosen as described in ref 34. The signal from silver coated with OOTF was found to be stable only for relatively short times. This problem originates from the e-beam-induced damage to the OOTF. The results presented below were obtained from fresh samples whose exposure to the electron beam did not exceed 3 min.

In the second scheme, the experimental system as described in refs 35 and 36 was used. The slides coated with the OOTF were attached to a temperature-controlled holder and inserted into an ultrahigh-vacuum (UHV) chamber pumped to below 10^{-8} mbar by adsorption and ion pumps. The 223 nm (5.56 eV) light with a 10 ns pulse of energy 0.1 μJ was obtained by mixing the output of a frequency-doubled Nd:Yag pumped dye laser with a 1064 nm light from the Nd:Yag laser. The laser beam is introduced into the chamber, and after reflecting from the sample it exits through quartz windows. The photoelectron kinetic energy distribution was measured via the retarding field method[37] or by time-of-flight electron energy analyzer.[38] In the first method, a grid made of nickel was placed 3 mm in front of and parallel to the silver/OOTF-coated slide. The grid could be biased with a negative or positive voltage relative to the silver surface, which was kept at ground potential. The close proximity of the grid and the silver surface ensures high collection efficiency and unperturbed collection of low-energy electrons. This kind of plane-parallel detector collects electrons according to the part of their kinetic energy corresponding to the velocity component perpendicular to the surface, $E_\perp$. If a negative potential $-V$ is applied on the grid, electrons with $E_\perp < eV$ cannot pass the mesh and therefore do not reach the detector. A newly developed microsphere plate (MSP made by El-Mul, Israel) was placed 5 mm behind the grid and biased by 200 V relative to it. The MSP serves as an electron multiplier, in the same way as does a regular microchannel plate. An anode placed behind the MSP collected the amplified electron signal, which was processed by a gated integrator (Stanford Research Systems). The laser pulse intensity was kept low so that nonlinear effects were eliminated. The signal measured by the retarding field method is an integral of the emitted current over the emitted electron energy up to the energy corresponding to the voltage applied on the grid. Hence, by differentiating the signal with respect to grid voltage, the emitted electron energy distribution is obtained. Although the method is inherently of low resolution, it has the advantage of being sensitive to the low-energy electrons. The electron energy distributions obtained by both methods were consistent.

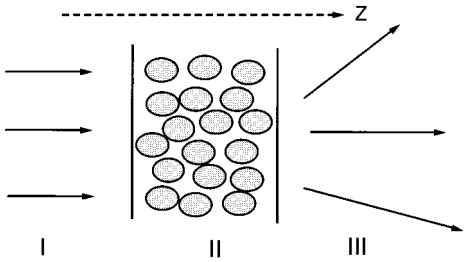

Figure 2. Schematic representation of electron transmission through a molecular film. An electronic plane wave (I) is incident on the barrier (II) from the left, and the transmission (III) is monitored from the right.

5. Computational Methods

Following the discussion of section 3, we need to compute transmission probabilities of either the "one-to-all" or the "cumulative" type. This is in principle a three-dimensional under-barrier tunneling or over-barrier transmission problem. Figure 2 depicts a typical one-to-all example: an electronic plane wave is incident on the barrier from the left, and the transmission (into all exit directions) is monitored on the right. The corresponding cumulative transition probability involves a sum over all incident directions l. For a nonuniform initial angular distribution, this sum should include a corresponding weight function. The computational problem can be quite challenging, in particular in situations where the barrier is very high so that

the transmission probability is very low. A prerequisite to any numerical treatment is a knowledge of the electron−barrier interaction. This is never known exactly in any realistic case, and two approximations have been used:

(1) A pseudopotential is constructed for the interaction of the electron with different atomic cores of the molecular layers. Such potentials have been constructed and successfully used in studies of energetics and dynamics of excess electrons in water,[39,40] ammonia[41], methanol[42], rare gases,[43] and simple alkanes.[44] Obviously such an approach can be valid only if the process under study involves only the excess electron, while the core electrons are taken care of only indirectly via the pseudo-potential. This can be true only in hosts with closed electronic shells and high electronic excitation and ionization energies. Once a suitable pseudopotential is available, the potential barrier for the electron transmission can be constructed if we assume that the total potential experienced by the electron as it moves from region I to III in Figure 2 is the sum of the potential experienced by the electron in the absence of the molecular layer ("the vacuum potential") and the potential associated with the electron−molecule interaction. The Schrödinger equation associated with the resulting one-electron Hamiltonian is then expressed on a grid spanning regions I, II, and III, and the transmission can be computed either as an initial value problem starting from a suitable wave packet on the left or as a scattering problem. We have found the latter formalism particularly useful, using the imaginary boundary conditions in Green's function method of Seidman and Miller.[45] In this method the potential is supplemented with an imaginary function of position along the transmission direction, $V \rightarrow V + i\epsilon(z)$, where $\epsilon(z)$ is taken to vary smoothly from zero in most of the bulk of the system to some suitably chosen large value near the edges. The cumulative transmission probability is then given by[45]

$$N(E) \equiv \sum_l \sum_r |S_{lr}(E)|^2 = 4tr[(1-h)\epsilon G h \epsilon G^*] \qquad (9)$$

where $h(z)$ is a step function, $h(z < 0) = 0$, $h(z \geq 0) = 1$, and G is the Green's operator

$$\hat{G}(E;\epsilon) = \frac{1}{E - \hat{H} + i\hat{\epsilon}(\mathbf{r})} \qquad (10)$$

Similarly, the "one-to-all" transmission probability is then calculated from

$$P_l(E) \equiv \sum_r |S_{lr}(E)|^2 = \langle \psi_l^+ | \hat{F} | \psi_l^+ \rangle \qquad (11)$$

where $\psi_l^+ = (E - H + i\epsilon)^{-1} i\epsilon\phi_l$, with ϕ_l being the incident state, and where $\hat{F} = i\hbar^{-1}[H, h(z)]$ is the flux operator. Obviously, the applicability of the above expressions depends on our ability to evaluate the grid Green's function in an efficient and accurate way (see methods reviewed in ref 46). In general, the size of a typical problem requires the use of iterative methods for the matrix inversion, and the calculation is facilitated by the fact that the Hamiltonian matrix defined on the grid is sparse.

(2) A finite basis set $\{m\}$ is constructed for the electron in the barrier region, and, for metal junctions, sometimes also for finite parts of the adjacent regions I and III. The basis functions and the associated Hamiltonian ($H_{mm'} = \langle m|H|m' \rangle$) and overlap ($S_{mm'} = \langle m|m' \rangle$) matrix elements are usually obtained in terms of the appropriate atomic orbitals within the extended Hückel formalism. The infinite nature of the system in the direction of the transmission is represented by assigning appropriate decay widths and level shifts to basis functions associated with some of the molecular centers. The cumulative and the "one-to-all" transmission probabilities are given by[47−52]

$$N(E) = 2\pi(\rho_L \rho_R |T_{lr}|^2)_{E_r = E_j = E} \qquad (12)$$

and

$$P_l(E_l) = 2\pi(\rho_R |T_{lr}|^2)_{E_r = E_l} \qquad (13)$$

respectively, where

$$T_{lr} = V_{lr} + \sum_m \sum_{m'} V_{lm} G_{mm'} V_{m'r} \qquad (14)$$

$$G = (E(I+S) - H - \Sigma(E))^{-1}; \quad \Sigma(E) = \Delta(E) - (1/2)i\Gamma(E) \qquad (15)$$

Here l and r denote states in the unspecified continuous manifolds (with density of states ρ_L and ρ_R respectively) on the left and on the right of the barrier respectively, and $\{m\}$ are the intermediate states that are considered explicitly. Σ is the self-energy matrix (with Δ and $(1/2)\Gamma$ its real and imaginary parts) of the molecular basis $\{m\}$ associated with its coupling to these manifolds. The coupling elements V_{lr} V_{lm} V_{mr} connect the molecular manifold to the continua of incoming and outgoing states and can be calculated or approximated within specified models of these continua. Again, when the number of orbitals associated with the intermediate state manifold is large, iterative inversion is the method of choice for evaluating the Green's function.

The two approaches described above differ from each other mostly in the basis functions used to describe the transmission process and also in the philosophy behind the corresponding descriptions. The molecular basis approach is useful when the transmission is supported by well-defined intermediate states ("through bond transfer") even though direct coupling can be accommodated, e.g., the first term on the right of (14) ("through space transfer"). The spatial grid approach is more useful when the transmission is not dominated by specific intermediate molecular states or when through space coupling dominates. Thus, in the simulations of transmission through water and argon layers described below, a pseudo-potential/spatial grid technique was found to be very useful.

6. Experimental Results

Figure 3 (Figure 3 in ref 35) presents the electron energy distribution of photoelectrons from silver coated with one (A), three (B), and five (C) monolayers of CdSt, $[(CH_3(CH_2)_{16}COO^-)_2Cd^{2+}]$. The importance of film order to electron transmission is demonstrated in Figure 4 (Figure 3 in ref 34), which presents the current density as function of electron energy, for photoelectrons transmitted through 13 layers of Cdar, $[(CH_3(CH_2)_{18}COO^-)_2Cd^{2+}]$, before (circles) and after (squares) they were heated to 378 K. The results indicate that before heating, electrons with energies above ca. 1eV are transmitted through the band almost ballistically. Following the heating, the electron energy distribution indicates an extensive scattering process.

When the SEE peak was monitored for surfaces covered with OOTF, it was found to be narrower than the peak for the bare substrate. The results are presented in Figure 5 (Figure 1 in ref 34) as the transmission function through one (solid line) and three (dashed line) layers of Cdar. The transmission curve

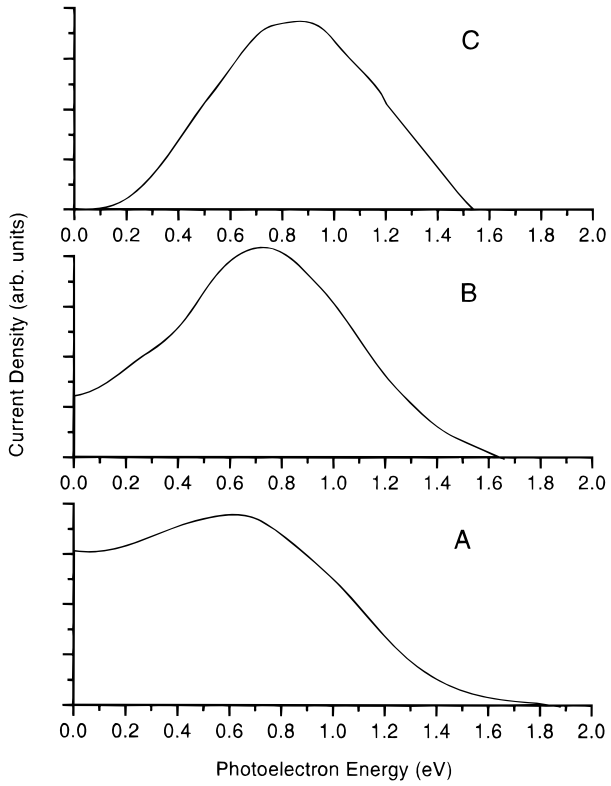

Figure 3. Electron energy distribution of photoelectrons from silver coated with one (A), three (B), and five (C) monolayers of cadmium stearate.

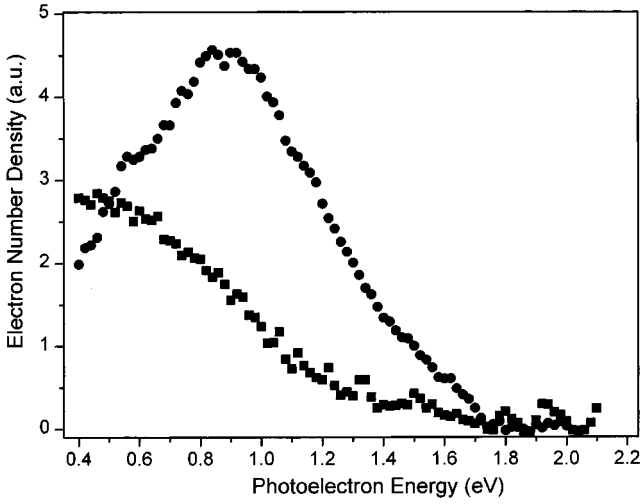

Figure 4. Electron energy distribution as measured by the retarding field method for photoelectrons transmitted through 13 organized (circles) and unorganized (squares) layers of Cdar.

was calculated by dividing the electron signal at each electron energy, obtained from silver film coated with the OOTF, by the electron signal of the bare silver film.

The low-energy part (<1 eV) of the curve obtained in this way is consistent with the results obtained by the retarding field method monitoring low-energy electrons, whereas at higher energies new information is obtained. One observes a decrease in the transmission probability for electrons with energy of above ca. 1.0 eV. This decrease is more abrupt, in terms of energies, when the film is composed of more layers.

Another aspect of the interplay between film structure and its transmission properties is shown in Figure 6, which presents the transmission probability of electrons as a function of the photoelectron energy for layers of Cdar (dashed), CdBr (dotted), and of mixed layers (solid) for three (Figure 6a) and nine (Figure 6b) layers. As is clearly evident, the electron transmission through the mixed layers is significantly less efficient than that through the Cdar or CdBr layers themselves. Not only is the transmission intensity reduced, but the energy distribution is also different. While the energy distribution for electrons transmitted through three layers of Cdar or CdBr peaks at 0.8 and 0.7 eV, respectively, the electron energy distribution of

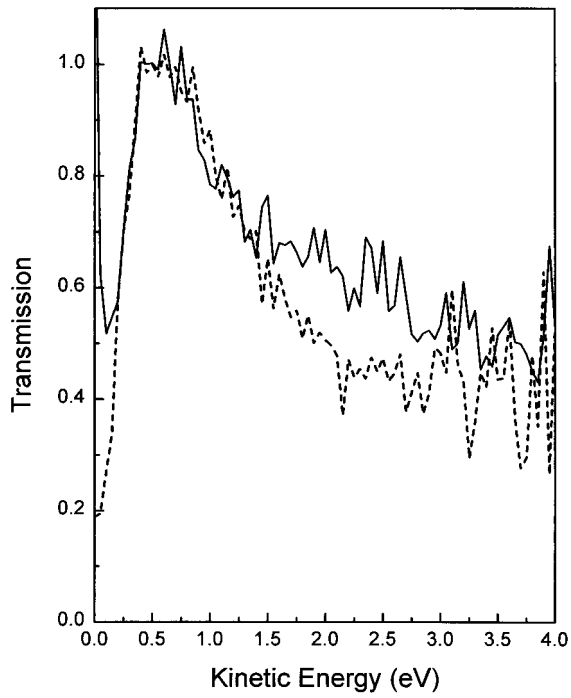

Figure 5. Transmission probability of photoelectrons through one (solid line) and three (dashed line) layers of Cdar.

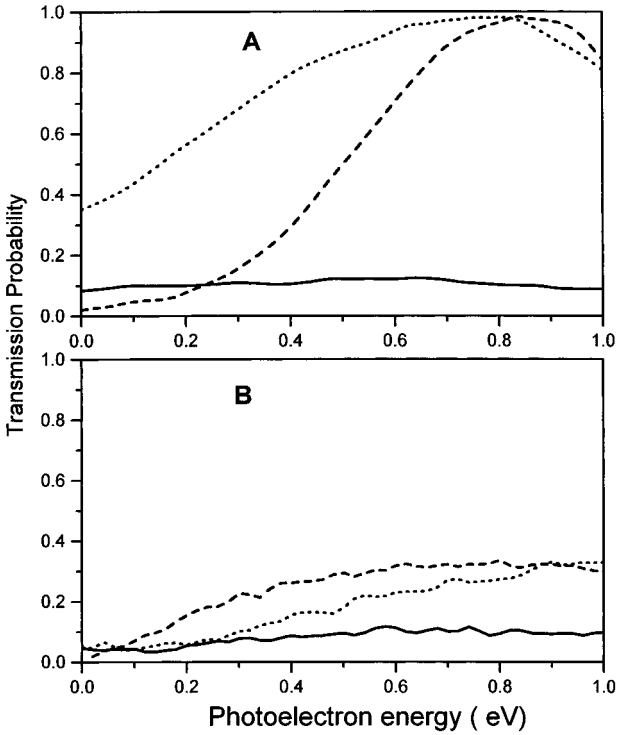

Figure 6. Transmission probability of electrons as a function of the photoelectron energy for layers of Cdar (dashed) and CdBr (dotted), and of mixed layers (solid) for three (A) and nine (B) layers.

electrons transmitted through the mixed layers is almost flat. In the case of the nine layered samples, the energy distribution of electrons transmitted through layers of Cdar or CdBr layers peaks at 0.7 and 0.9 eV, respectively. Generally, in the case of nine layers, less electrons are transmitted through the film.

Figure 6 shows that in the case of the neat films, namely, films of either Cdar or CdBr alone, electrons with energies above some threshold value (V_0) are transmitted almost unperturbed, while the transmission is lower for low-energy electrons. This type of energy-dependent transmission indicates the existence of band structure in the film, as was discussed above, with the bottom of the conduction band at V_0. However, the distribution of electrons transmitted through the mixed layer indicates an extensive scattering process incompatible with the band model. This means that despite the fact that the order and packing of the layers is very similar for all three type of layers used (Cdar, CdBr, and mixed layers), the fact that in the mixed layers case not all the chains are identical, this fact by itself, causes the reduction in electron transmission.

Some word of caution is in place at this point. The notion of electronic bands is of course related to the electronic structure of ordered bulk solids, and applying it to thin films is in principle questionable. Indeed, it is sufficient to associate high transmission probabilities with states of the excess electron in the film that are extended on the scale of the film thickness. In fact, the numerical results presented below suggest that the correspondence with the band structure of the bulk material is substantial even for very thin films.

7. Some Numerical Results

While the numerical methodologies described in section 3b are general and can in principle be applied to the experimental systems described above, the numerical results described below are used to illustrate the principle factors affecting the transmission using simpler model systems. We consider (a) the dimensionality of the process, (b) the effect of layer structure and order, (c) the effect of resonances in the barrier, and (d) the signature of band motion. Details of the pseudopotentials, grids, basis sets, and matrix elements are provided in the corresponding references. It should be emphasized that even though the systems so far studied numerically are very different than the organized organic layers that are the subjects of our experimental work, these factors and the way they affect the transmission characteristics appear to be general.

Many theoretical studies of tunneling use one-dimensional models, the rationale being that a process dominated by nonresonance tunneling, and therefore exponentially diminishing with tunneling path length, must take the shortest possible route. Figure 7 (Figure 6 of ref 46) shows that the situation is more complex. This figure shows the "one-to-all" tunneling probability for an electron incident in the normal direction on a 1.0 nm layer of water. In this calculation water configurations are obtained from classical trajectories at 300 K, and the electron water pseudo-potential is the one developed by Barnett et al., which uses a two-body term to account for the water electronic polarizability. This pseudo-potential is superimposed on a vacuum potential modeled by a rectangular barrier of height 5 eV and width 1.0 nm. Figure 7 compares the result of a full 3-D calculation to that obtained as an average over 256 one-dimensional paths through the same water configurations. The resulting relatively large one-dimensional transmission was found to be dominated by just a few paths with very low barriers. These paths are embedded as very narrow potential windows in the three-dimensional water configuration. In a 3-D calculation tunneling through these paths is suppressed by a very high kinetic energy barrier, hence the actual 3-D tunneling probability is much smaller.

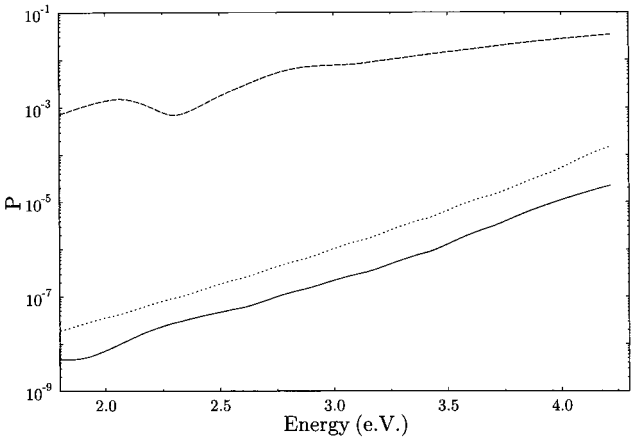

Figure 7. Tunneling probability vs electron energy through a film of water molecules. The film thickness is ~10 Å, and the water density is ~1 g/cm^3, which amounts to three monolayers of water in the film. The water−electron potential is superimposed on a "vacuum barrier" of height 5 eV. The nonpolarizable electron−water pseudo-potential of Barnett et al.[39] is used here (see ref 46 for more details). Full line: Tunneling probability vs electron energy calculated for a particular three-dimensional water configuration in the barrier. Dashed line: Average over 256 tunneling probabilities calculated for linear one-dimensional sections through the same barrier. Dotted line: Tunneling probability through the bare rectangular barrier of height 5 eV.

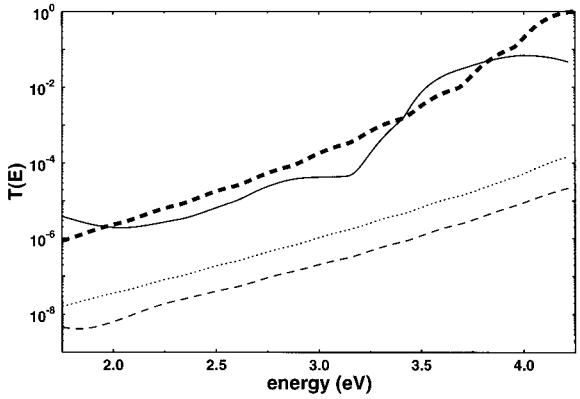

Figure 8. Tunneling probability vs electron energy calculated for a particular three-dimensional water configuration in the barrier (same barrier as in Figure 7). Dotted line: tunneling through the vacuum barrier. Thin dashed line: tunneling through the water film, using the nonpolarizable electron−water pseudo-potential. (These two lines appear also in Figure 7.) Full line: tunneling through the same water film, using the fully polarizable electron−water interaction (see ref 53 for details). The thick dashed line represents the tunneling probability calculated for a rectangular barrier of width 10 Å and height 3.8 eV.

It should be noted that while Figure 7 shows quite dramatically the importance of taking the correct dimensionality of the system into account, the absolute results for electron tunneling through water do not account for experimental observations. Experiments indicate that the effective barrier to tunneling in water is considerably lower (by ~1 eV) than in vacuum, while the results of Figure 7 show a different trend. We have found that the problem originates from disregarding the electronic polarizability of water in the water−electron pseudo-potential. This is shown in Figure 8 (Figure 3 of ref 53) where the predictions of the polarizable and nonpolarizable models of the electron−water pseudo-potential are compared. The polarizable model accounts quite well for the observed reduction in the

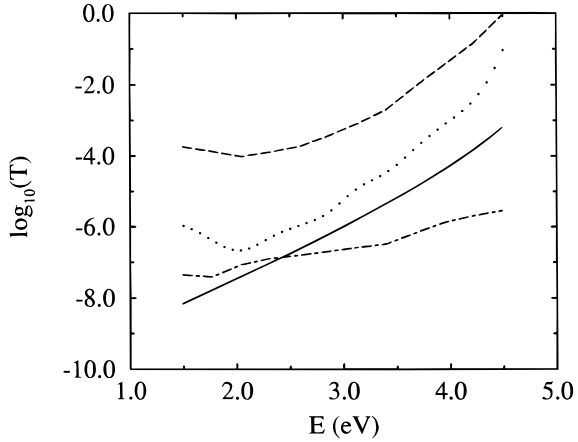

Figure 9. Computed tunneling probability through 10 Å water layers. Dotted line: normal equilibrium configuration obtained from MD simulations at 300 K. Dashed line: configurations in which the water molecules are oriented so that their dipoles are pointing opposite to the tunneling direction. Dashed−dotted line: same where the water dipoles point in the tunneling direction. The full line is the vacuum (no water) tunneling probability. (See ref 54 for more details.)

effective barrier to tunneling in water as compared with vacuum.

Another demonstration of the importance of the 3-D structure of the water layer on the characteristic of the tunneling process is shown in Figure 9 (Figure 3 of ref 54). Here, using the polarizable model for the electron−water interaction we show the "one-to-all" transmission probability for an electron incident in the normal direction on a 1.0 nm water layer in which the water molecules are oriented in the tunneling direction by a strong electric field. This figure compares the vacuum tunneling to tunneling through a normal water layer and through a similar water layer oriented in the opposite to the tunneling direction. We emphasize that the strong asymmetry predicted cannot be obtained in a one-dimensional calculation because of constraints imposed by microscopic reversibility.

In a molecular layer made of adsorbed chain molecules, the dimensionality issue can be expressed with a slightly different emphasis: does the transmission occur predominantly along single chains or do cross-interactions between chains affect it in an essential way? This is obviously an issue of interaction strengths and distances and should be studied using detailed models. As a demonstration of the effects of cross-chain interactions, we show in Figure 10 the result of a two-dimensional calculation of the transmission of an electron incident in a perpendicular direction on a barrier in which two chains of wells lie parallel to each other in the direction of transmission. The rectangular barrier height is 0.1 au, and its width in the tunneling direction is 36 au. Each "chain" is made of wells of size 4 × 4 au, lying at a distance of 8 au between their centers. Figure 10 shows the ratio $T_2/(2T_1)$ between the computed transmission probability T_2 and twice the transmission probability associated with an isolated chain as a function of the interchain distance. This ratio should be approximately 1 if cross-chain interactions are absent and if through-wells transmission dominates. We see that for the parameters chosen, interchain interactions become important at distances smaller than 15 au. We may conclude that such effects may be important at molecular distances for normal hydrocarbon layers.

Finally, consider ordered vs disordered layer structure. Figure 11 (Figure 2 of ref 34) compares the transmission probability ("one-to-all" with the incident electron perpendicular to the barrier; note that a complete solution of the transmission problem corresponds to averaging the transmitted flux over the angular

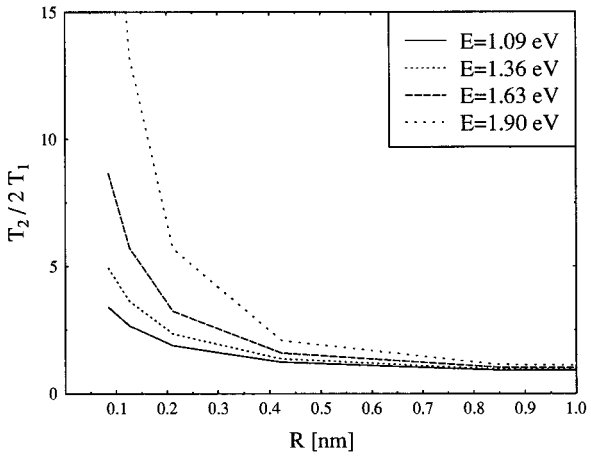

Figure 10. Two-dimensional model calculation of the transmission of an electron incident in a perpendicular direction on a rectangular barrier in which two chains of wells lie parallel to each other in the direction of transmission. The rectangular barrier height is 0.1 au, and its width in the tunneling direction is 36 au. Each "chain" is made of wells of size 4 × 4 au and depth below the barrier of 0.05 au, lying at a distance of 8 au between their centers. Plotted as a function of the interchain distance and for different electron energies is the ratio $T_2/(2T_1)$, where T_2 is the computed transmission probability and T_1 is the transmission probability for a single chain.

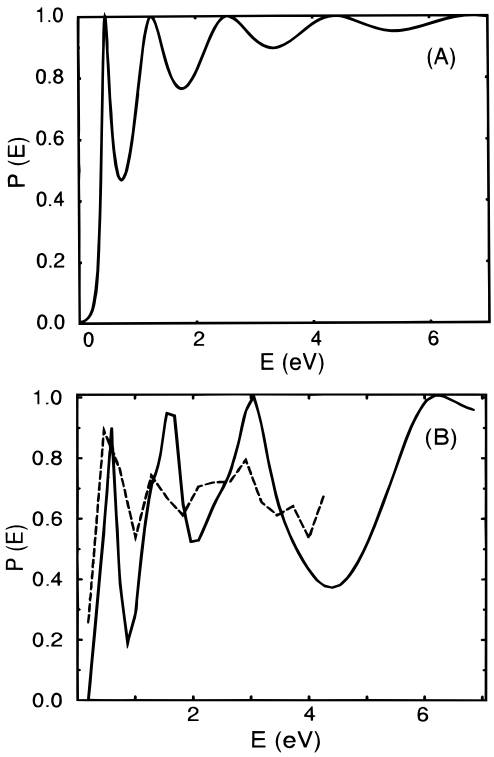

Figure 11. (a) Transmission probability through 1-D rectangular barrier characterized by height of 3 eV and width of 12 Å, as a function of incident electron energy measured relative to the barrier top. (b) Full line: electron transmission through a slab made of four Ar layers, cut out of an fcc Ar crystal in the (100) direction. Dashed line: same results obtained for a disordered Ar slab prepared as described in the text.

distribution of the incident electrons) through a one-dimensional rectangular barrier of height 3 eV and width 1.2 nm as a function of the incident electron energy measured relative to the barrier top, to the transmission through a 3-D slab of four Ar layers cut out of an Ar crystal in the (100) direction. The latter results are obtained with a spatial grid technique using the electron−Ar pseudo-potential of Space et al.[43] The oscillations shown

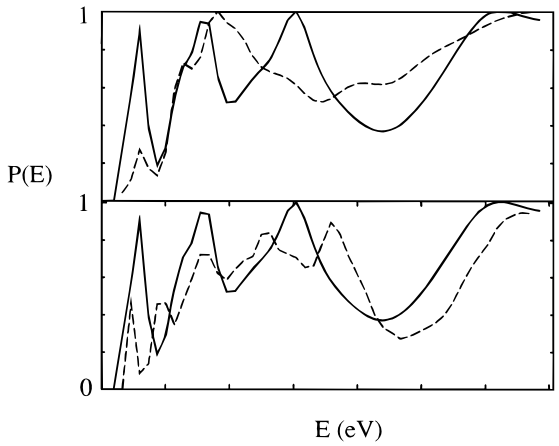

Figure 12. Computed transmission probabilities, vs electron energy, for an electron incident on slabs cut out of an fcc Ar crystal in the (100) direction. (a) Slabs made of two (dashed line) and four (full line) monolayers. (b) Slabs with four (full line) and six (dashed line) monolayers. (The full lines in (a) and (b) are identical.)

in Figure 11a are interference patterns associated with the finite width of the layers. The full line in Figure 11b also shows such oscillations, but in addition, a prominent dip above 4 eV corresponds to a band gap, already well-developed in this thin ordered layer. The dashed line in Figure 11b shows similar transmission results for disordered layers, obtained from the crystalline layer by a numerical thermal annealing at 400 K next to an adsorbing wall using molecular dynamics propagation. The results shown are averaged over four such disordered Ar configurations. The transmission through the disordered layer is considerably less structured (very likely, smoother shapes will be obtained with more configurational averaging); in particular, the dip associated with the band gap has largely disappeared.

Another issue of interest is the development of the band structure as the film thickness increases. Figure 12 compares the transmission (one-to-all) versus electron energy, for an electron incident in the normal direction on ordered Ar films made of two, four, and six atomic monolayers ("prepared" by cutting them off an Ar crystal as described above). Already at six-layer thickness the observed transmission dip is very close to its bulk value, indicating that the band structure is already well-developed.

The examples described above have used the imaginary boundary conditions Green's function/spatial grid technique to evaluate the transmission probability. In the case of transmission through organic layers, the proximity of molecular orbitals to the energy of the transmitted electron suggests that the approach based on a molecular basis set may be better and more efficient. Recent model calculations of the conductivity of carbon chains and of STM images of organic molecules[47,48,50−52,55−62] on metal substrates show the viability of this approach. Applications of this method to adsorbed chain molecules are currently underway.

8. Discussion

Electron transmission through organized organic thin films depends sensitively on details of the composition and structure of the film and on the nature of the substrate. Still the result presented above show several modes of behavior, which, in comparison with the model calculations, are expected to be general. While the model computations described above are not dealing yet with the actual experimental systems, they do show generic characteristics of these processes. These are (a) the three-dimensional character of the transmission process and (b) the dependence on the electronic band structure of the underlying bulk molecular solid.

Dimensionality Issues. Because of the exponential damping of tunneling probability with barrier width, it is tempting to regard the electron transfer as a one-dimensional process, and in fact theoretical discussions of electron transfer often use such models. For overbarrier transmission (or for electron transport through extended electronic states in the barrier, e.g., through conduction band states) this argument does not apply, and the transmission probability may be affected by the full three-dimensional structure of the molecular film. Even in this case the relative importance of conduction along the backbone of a single chain molecule and of interchain coupling is an interesting issue. The computational results displayed in Figures 7 and 9 clearly indicate that even for deep tunneling processes 1-D models are generally inadequate and may miss important physical aspects of the process. No detailed calculations for transmission through organized layers made of chain molecules are available yet; however, the model calculation of Figure 10 demonstrates how interchain effects may come in as the distance between molecular chains decreases. In accordance with these observations, the experimental results in Figure 6 show that not only the structure of the dielectric in the direction of propagation (*Z*-direction) of the electron but also its structure in the perpendicular XY plane are important in determining the transmission probability. This observation is significant because each chain considered independently is a periodic structure which could support one-dimensional band conduction. Still, the DeBroglie wavelength (≈1.2 nm for electron energy of 1 eV) is longer than the spacing between chains and an electron moving in the *Z*-direction samples the potential from neighboring chains so its motion can be sensitive to disorder in the *XY*-plane. Indeed, Figure 6 shows that lateral disorder in the potential, in the case of the mixed layers, is enough of a perturbation to decrease the efficiency of electron transmission.

Band Structure Effects. The transmission of an electron through a molecular film depends on the electronic structure of the film, in the same way that bridge assisted electron transfer is dominated by the electronic structure, particularly LUMOs (lowest unoccupied molecular orbitals) of the bridge. It should be kept in mind that the relevant electronic states in the present context are *excess electron states* in the film. For ordered molecular layers such states may be extended, at least on the scale of the film thickness, and constitute the precursor of what would become the conduction band in the macroscopic bulk solid. Band structure effects have been indeed seen in the LEET experiments of Sanche and co-workers.[18] The consequences of such band motion are seen also in the experimental and numerical results presented above. It is interesting to note (Figures 11 and 12) that signature of the bulk band structure is seen even for very thin Ar layers; in fact, even a film consisting of two atomic monolayers shows a structure that can be identified as the precursor of the bulk band gap (Figure 12). For the Cdar system, even a monolayer is considerably thicker than the simulated system, so we expect that the energy dependence of the transmission through such layers will be dominated by the electronic band structure and/or impurity and defect states in these layers. X-ray studies indicate that, at room temperature, three layers of Cdar or more show clear crystalline diffraction, while a single layer is less ordered.[63] Hence it is expected that the band structure in the three-layer system will be better defined, as indeed indicated by the sharper transmission peak for electrons transmitted through three Cdar layers,

compared to those transmitted through a single layer (Figure 5). Furthermore, the orthorhombic crystalline structure of the Cdar film is destroyed upon heating the films to 378 K, and the amphiphilic chains are not ordered above this temperature.[63] From Figure 4 it is evident that after heating there is an efficient scattering process that suppresses the transmission peak similarly to what is observed in the calculated dashed line of Figure 11b.

These results indicate that "band conduction", or transmission through electronic states which are extended at least along the film normal, is the cause of the efficient electron transmission through amphiphiles. This picture also explains the high conductance through organic layers as measured with scanning tunneling microscopy.[64] It also rationalizes the observation that electrons are better conducted through all-trans amphiphilic chains than through chains containing some gauche bonds:[65] When the chains are in "all-trans" configuration, the layer is ordered and the electronic wave functions in the band are delocalized. The formation of the gauche bonds amounts to introducing disorder which increases scattering and reflection and, when pronounced enough, localizes the electronic wave function.

It is also important to note that the observed role of bandlike motion in the electron-transmission process indicates that classical multiple scattering approaches to such processes are inadequate and emphasizes the importance of treating the electron-transmission quantum mechanically.

As discussed in section 3, the electron-transmission processes that were the focus of the present work are closely related to the general class of electron-transfer phenomena. Following Marcus,[66] most treatments of electron transfer focus on the electronic states of the donor and acceptor species, treating the surrounding solvent as a dielectric continuum. By its very nature, the study of photoemission through molecular overlayers focuses on the molecular structure of these layers, the equivalents of the bridge and solvent in other electron-transfer processes. We have already commented on the analogy between transmission through such layers and between bridge-assisted electron-transfer processes, and experiments of the kind described here focus directly on the effect of the electronic structure of such (three-dimensional) bridges. It is possible from the photoelectron transmission studies and from LEET to obtain the effective barrier height and the energy-dependent transmission probability through such bridges, information which is not directly available in other types of electron-transfer processes. Current studies in our laboratories aim at establishing if and how the character (angular distribution, momenta, polarization etc.) of the electrons affect the transmission probabilities.

Acknowledgment. This work was partially supported by the Ministry for Science and Technology and by the United States−Israel Binational Science Foundation. R.N. thanks the partial support from the Israel Science Foundation and from the MINERVA Foundation.

References and Notes

(1) Kuznetsov, A. M. *Charge Transfer in Physics, Chemistry and Biology*; Gordon and Breach: New York, 1995.

(2) (a) Carter, F. L. *Molecular Electronic Devices*; Marcel Dekker Inc.: New York, 1987; Vol. 2. (b) Lehn, J. M. *Angew. Chem.* **1988**, *100*, 89. (c) *Molecular and Biomolecular Electronics*; Birge, R. R., Ed.; American Chemical Society: Washington DC, 1994. (d)Aviram, A.; Ratner, M. A. *Chem. Phys. Lett*. **1974**, *29*, 277.

(3) *Molecular Electronics*; Jortner, J., Ratner, M., Eds.; Blackwell Science Ltd: Oxford, 1997.

(4) Sanche, L. *Scanning Microsc.* **1995**, *9*, 619.

(5) Barraud A.; Millie P.; Yakimenko I. *J. Chem. Phys.* **1996**, *105*, 6972 and references cited therein.

(6) (a) A. Ikai, *Surf. Sci. Rep.* **1996**, *26*. (b) DeRose, J. A.; Leblanc, R. M. *Surf. Sci. Rep.* **1995**, *22* and references cited therein.

(7) Wolf, E. L. *Principles of electron tunneling spectroscopy*; Oxford University Press: Oxford, 1985.

(8) Gurney, R. W. *Phys. Rev.* **1935**, *47*, 479.

(9) Ueba, H. *Surf. Sci.* **1991**, *242*, 266.

(10) Albano, E. V. *Appl. Surf. Sci.* **1982**, *14*, 183.

(11) Lang, N.; Kohn, W. *Phys. Rev. B* **1970**, *1*, 4555.

(12) Duwez A.-S.; Paolo S. D.; Ghijsen J.; Riga J.; Deleuze M.; Delhalle J. *J. Phys. Chem. B* **1997**, *101*, 884.

(13) Jo, S. K.; White, J. M. *J. Chem. Phys.* **1991**, *94*, 5761.

(14) Michaud, M.; Sanche, L. *Phys. Rev.* **1987**, *A36*, 4672.

(15) Kim, C.-W.; Villagran, J. C.; Even, U.; Thompson, J. C. *J. Chem. Phys.* **1991**, *94*, 3974.

(16) Petrank, A. Ph.D. Thesis, Weizmann Institute of Science, 1987.

(17) For a review, see: Sanche, L. In *Excess Electrons in Dielectric Media*; Ferradini, C.; Jay-Gerin, J.-P., Eds.; CRC Press: Boca Raton, FL, 1991; Chapter 1, p 1.

(18) Perluzzo, G.; Bader, G.; Caron L. G.; Sanche, L. *Phys. Rev. Lett.* **1985**, *55*, 545.

(19) Caron, L. G.; Perluzzo, G.; Bader, G.; Sanche, L. *Phys. Rev. B* **1986**, *33*, 3027.

(20) Maeda, T.; Miyano, K.; Sugita, K.; Ueno, N. *Thin Solid Films* **1989**, *179*, 327. Ueno, N.; Nakahara, H.; Sugita, K.; Fukuda, K. *Thin Solid Films* **1989**, *179*, 161. Ueno, N.; Sugita, K. *Phys. Rev. B* **1990**, *42*, 1659.

(21) Bader, G.; Perluzzo, G.; Caron, L. G.; Sanche, L. *Phys. Rev.* **1984**, *B30*, 78.

(22) (a) Michaud, M.; Sanche, L.; Gaubert, C.; Baudoing, R. *Surf. Sci.* **1988**, *205*, 447. (b) Goulet, T.; Jung, J.-M.; Michaud, M.; Jay-Gerin, J.-P.; Sanche, L. *Phys. Rev.* **1994**, *B50*, 5101.

(23) Vincett, P. S.; Roberts, G. G. *Thin Solid Films* **1980**, *68*, 135 and references cited therein.

(24) Polymeropoulos, E. E.; Sagiv, J. *J. Chem. Phys.* **1978**, *69*, 1836.

(25) Landauer, R. IBM *J. Res. Dev.* **1957**, *1*, 223.

(26) Landauer, R. *Philos. Mag.* **1970**, *21*, 863.

(27) Imry, Y. Physics of mesoscopic systems. In *Directions in Condensed Matter Physics*; Grinstein, G., Mazenko, G., Eds.; World Scientific: Singapore, 1986; p 101.

(28) M. Galperin, D. Segal, and A. Nitzan, to be published.

(29) A. Haran, S. P. Ananthavel, and R. Naaman, in preparation.

(30) Blodgett, K. B. *J. Am. Chem. Soc.* **1935**, *57*, 1007. Blodgett, K. B.; Langmuir, I. *Phys. Rev.* **1937**, *51*, 964.

(31) Kadyshevitch A.; Ananthavel S. P.; Naaman R. *J. Chem. Phys.* **1977**, *107*, 1288.

(32) Popovitz-Biro, R.; Wang, J. L.; Majewski, J.; Shavit, E.; Leiserovitch, L.; Lahav, M. *J. Am. Chem. Soc.* **1994**, *116*, 1179.

(33) Trakhtenberg S.; Naaman R.; Cohen S. R.; Benjamin I. *J. Phys. Chem.* **1997**, *101*, 5172.

(34) Haran A.; Kadyshevitch, A.; Cohen, H.; Naaman, R.; Evans, D.; Seidman, T.; Nitzan, A. *Chem. Phys. Lett.* **1997**, *268*, 475.

(35) Kadyshevitch A.; Naaman R. *Phys. Rev. Lett. 74*,3443.**1995**, .

(36) Kadyshevitch A.; Naaman R. *Thin Solid Films* **1996**, *288*, 139.

(37) DuBridge, L. A. *Phys. Rev.* **1933**, *43*, 727.

(38) We thank Prof. O. Cheshnovsky for advising us on the construction of the time-of-flight spectrometer.

(39) Barnett, R. N.; Landmann, U.; Cleveland, C. L. *J. Chem. Phys.* **1988**, *88*, 4420.

(40) Rossky, P. J.; Schnitker, J. *J. Phys. Chem.* **1988**, *92*, 4277.

(41) Sprik, M.; Klein, M. L. *J. Chem. Phys.* **1988**, *89*, 1592.

(42) Turi, L.; Mosyak, A.; Rossky, P. J. *J. Chem. Phys.* **1997**, *107*, 1687.

(43) Space, B.; Coker, D. F.; Liu, Z. H.; Berne, B. J.; Martyna, G. *J. Chem. Phys*. **1992**, *97*, 2002.

(44) Liu, Z.; Berne, B. J. *J. Chem. Phys.* **1993**, *99*, 9054.

(45) Seidman, T.; Miller, W. H. *J. Chem. Phys.* **1992**, *97*, 2499.

(46) Mosyak, A.; Nitzan, A.; Kosloff, R. *J. Chem. Phys.* **1996**, *104*, 1549.

(47) Mujica, V.; Kemp, M.; Ratner, M. A. *J. Chem. Phys.* **1994**, *101*, 6849, 6856.

(48) Kemp, M.; Roitberg, A.; Mujica, V.; Wanta, T.; Ratner, M. A. *J. Phys. Chem.* **1996**, *100*, 8349.

(49) Samanta, M. P.; Tian, W.; Datta, S.; Henderson, J. I.; Kubiak, C. P. *Phys. Rev. B* **1996**, *53*, R7626.

(50) Sautet, P.; Joachim, C. *Phys. Rev. B.* **1988**, *38*, 12238.

(51) Sautet, P.; Joachim, C. *Chem. Phys. Lett.* **1991**, *185*, 23.

(52) Joachim, C.; Gimzewski, J. K.; Schlittler, R. R.; Chavy, C. *Phys. Rev. Lett.* **1995**, *74*, 2102.

(53) Mosyak, A.; Graf, P.; Benjamin, I.; Nitzan, A. *J. Phys. Chem. A* **1997**, *101*, 429.

(54) Benjamin, I.; Evans, D.; Nitzan, A. *J. Chem. Phys.* **1997**, *106*, 1291.

(55) Chavy, C.; Joachim, C.; Altibeli, A. *Chem. Phys. Lett.* **1993**, *214*, 569.

(56) Cheong, A.; Roitberg, A. E.; Mujica, V.; Ratner, M. A. *J. Photochem. Photobiol. A* **1994**, *82*, 81.

(57) Joachim, C.; Gimzewski, J. K. *Europhys. Lett.* **1995**, *30*, 409.
(58) Kemp, M.; Mujica, V.; Ratner, M. A. *J. Chem. Phys.* **1994**, *101*, 5172.
(59) Mujica, V.; Kemp, M.; Ratner, M. A. *J. Chem. Phys.* **1994**, *101*, 6856.
(60) Sautet, P.; Dunphy, J. C.; Ogletree, D. F.; Joachim, C.; Salmeron, M. *Surf. Sci.* **1994**, *315*, 127.
(61) Sautet, P.; Joachim, C. *Chem. Phys. Lett.* **1988**, *153*, 511.
(62) Sautet, P.; Joachim, C. *Chem. Phys.* **1989**, *135*, 99.
(63) Tippmann-Krayer, P.; Kenn, R. M.; Mohwald, H. *Thin Solid Films* **1992**, *210/211*, 577.
(64) DeRose, J. A.; Leblance, R. M. *Surf. Sci. Rep.* **1995**, *22*, 75.
(65) Haran, A.; Waldeck, D. H.; Naaman, R.; Moons E.; Cahen, D. *Science* **1994**, *263*, 948.
(66) Marcus, R. A. *Oxidases and Related Redox Systmes;* King T. E., Mason H. S., Morrison, M., Eds.; Pergamon Press: New York, 1982; p 3.